Solution Structure of the cAMP-Dependent Protein Kinase Catalytic Subunit and Its Contraction upon Binding the Protein Kinase Inhibitor Peptide†

G. A. Olah,‡ R. D. Mitchell,§ T. R. Sosnick,‡ D. A. Walsh,§ and J. Trewhella*,‡

Isotope and Nuclear Chemistry Division, Los Alamos National Laboratory, Los Alamos, New Mexico 87545, and Department of Biological Chemistry, University of California, Davis, California 95616

Received October 19, 1992; Revised Manuscript Received January 21, 1993

ABSTRACT: Small-angle X-ray scattering and Fourier transform infrared (FTIR) spectroscopy experiments have been completed on the catalytic subunit of the cAMP-dependent protein kinase. Measurements were made both with and without the protein kinase inhibitor peptide, PKIα(5–22)amide. Binding of the peptide results in an overall contraction of the structure that is characterized by a decrease of 9% in radius of gyration and about 16% in the maximum linear dimension. Both the secondary structure content of the protein/peptide complex, as determined by FTIR, and the solution structure of this binary complex, as determined by X-ray scattering, agree well with the structural characteristics of this complex as elucidated by the crystal structure [Knighton, D. R., Zheng, J., Ten Eyck, L. F., Ashford, V. A., Xuong, N.-H., Taylor, S. S., & Sowadsi, J. M. (1991a) *Science 253*, 407–414]. Further, the contraction of the structure observed by X-ray scattering upon inhibitor peptide binding is not accompanied by any detectable change in secondary structure content of the kinase. We have modeled the contraction of the kinase upon inhibitor peptide binding as a simple rotation of the large and small lobes seen in the crystal structure such that the cleft between them is closed. For a substrate these changes would then allow catalysis to ensue. The hinge for this movement occurs around a glycine that is one of the protein kinase family consensus amino acids.

The cAMP-dependent protein kinase is a member of a large family of protein kinases which catalyze the transfer of the terminal phosphoryl group from a nucleotide triphosphate to the hydroxyl group of serine, threonine, or tyrosine residues of target proteins (Hanks et al., 1988). It is currently the protein kinase about which most is known, and it thus serves as a model for other proteins of this gene family. PK is composed of four subunits: two identical catalytic subunits (M_r = 40 862) and two identical regulatory subunits (M_r = 45 084). The inactive holoenzyme is activated upon binding of two molecules of cAMP to each regulatory subunit leading to the dissociation of the holoenzyme into a regulatory-subunit dimer and two free catalytic subunits.

Recently, the three-dimensional structure of the cAMP-dependent protein kinase catalytic subunit (M_r 40 862) in binary complex with the high-affinity peptide PKIα(5–24)[1] derived from the protein kinase inhibitor protein (Walsh et al., 1990) has been elucidated at 2.7-Å resolution (Knighton et al., 1991a,b). The crystal structure shows the kinase to be composed of a large and a small lobe, with a cleft between these two domains containing the MgATP binding site and the residues involved in phosphotransferase activity. The protein kinase inhibitor peptides, PKIα(5–22)amide and PKIα(5–24), are high-affinity competitive inhibitors derived from PKIα, the specific inhibitor protein first isolated from rabbit skeletal muscle (Glass et al., 1989; Walsh et al., 1990). These peptides bind via interactions of the identified amino acids in the sequence ^{5}X-X-X-X-X-Phe-X-X-X-X-Arg-X-X-Arg-Arg-X-X-Ile^{22}, with specific docking determinants on the protein kinase (Walsh et al., 1992). This interaction models that of the binding by protein kinase substrates which frequently contain the motif Arg-Arg-X-Ser/Thr-H, where H indicates a hydrophobic residue and Ser/Thr is the phosphorylation site (Walsh et al., 1992). The pseudosubstrate C-terminal half of PKIα(5–22) has an Ala at position 21 instead of the Ser or Thr residue. It is of interest in this regard that the substituted peptide (Ser21)PKIα(14–22)amide is the most potent protein/peptide substrate of the cAMP-dependent protein kinase yet identified (Glass et al., 1989). The structure of the bound inhibitor peptide, as identified as X-ray crystallography of the binary complex, agrees well with that deduced from solution structure data of the peptide alone; in each the N-terminal residues form an α-helix followed by a 4-residue turn structure and the C-terminal half is a section of extended chain (Reed et al., 1989).

We have completed small-angle X-ray scattering and Fourier transform infrared (FTIR) spectroscopy experiments which allow us to compare the overall dimensions and secondary structure content of the solution and crystal forms of the protein kinase catalytic subunit–PKIα(5–22)amide binary complex and also to characterize the expansion of the protein kinase structure that occurs when the inhibitor peptide is removed. A preliminary report of this work has been previously presented (Mitchell et al., 1990).

MATERIALS AND METHODS

Sample Preparation. The catalytic subunit of the cAMP-dependent protein kinase was purified to homogeneity as described previously (Fletcher et al., 1986). The samples used for these studies were stored in 50% glycerol at 20 °C and used within two weeks of preparation. The inhibitor peptide PKIα(5–22)amide (Thr-Thr-Tyr-Ala-Asp-Phe-Ile-Ala-Ser-

† This work was performed under the auspices of the DOE (Contract W-7405-ENG-36) and was supported by NIH Grants GM40528 (J.T.) and GMK21019 (D.A.W.).

* To whom correspondence should be addressed.

‡ Los Alamos National Laboratory.

§ University of California.

[1] Abbreviations: d_{max}, maximum linear dimension; FTIR, Fourier transform infrared; PKI, cAMP-dependent protein kinase inhibitor protein; PKIα, the α isoform of PKI; PKIα(5–22)amide and PKIα(5–24)amide, peptides corresponding to residues 5–22 and 5–24 of PKI, respectively [PKIα and PKIβ are two isoforms of PKI (Van Patten et al., 1993), first identified in rabbit skeletal muscle (Walsh et al., 1990) and rat testis (Van Patten et al., 1991), respectively]; R_g, radius of gyration.

0006-2960/93/0432-3649$04.00/0

Gly-Arg-Thr-Gly-Arg-Arg-Asn-Ala-Ile-NH_2) was synthesized and purified as described previously (Glass et al., 1989). Protein stocks for FTIR and scattering experiments were stored in buffer A (5 mM Tris buffer, pH 7.4, 100 mM NaCl, 0.2 mM EDTA, 15 mM β-mercaptoethanol) and 50% (w/v) glycerol, at a concentration between 3 and 4 mg/mL. PKIα-(5–22)amide stocks were prepared as a concentrated solution, 6.38 mM, in H_2O, pH 6.8. For X-ray scattering, the stock solutions of the protein kinase were warmed to 4 °C approximately 2 h prior to the measurement, diluted with buffer A to give 10% glycerol, and then reconcentrated using a Centricon-30 to give a 3.38 mg/mL (0.083 mM) protein kinase solution. The kinase/inhibitor peptide was prepared by combining aliquots of the protein kinase solution with the PKIα(5–22)amide solution and 300 mM MES buffer, pH 6.8 (ratio of volumes were 9:1:1). Matching samples of the uncomplexed protein kinase were prepared similarly, by substituting H_2O for the PKIα(5–22)amide aliquot. Final samples for X-ray scattering were therefore 2.7 mg/mL (0.066 mM) protein kinase, with equimolar peptide if present, in 27.2 mM MES buffer, pH 7.4. Samples for FTIR measurement were prepared by dialysis of the stock protein kinase solution in 50% glycerol against a 25% glycerol solution with buffer A in D_2O containing fresh β-mercaptoethanol. The protein was then concentrated to 7.44 mg/mL using a Centricon-30. Peptide that had been exchanged into D_2O by repeated lyophilization was added to give a 1:1 molar stoichiometry. The final concentration of the kinase/inhibitor peptide complex was 0.16 mM in 27.2 mM MES buffer, 99.9% D_2O, pD 7.4 (uncorrected meter reading). Samples for buffer/background spectra for FTIR and for scattering were made carefully to match the respective samples using the flowthrough from the Centricon steps.

FTIR Spectroscopy. FTIR spectra were recorded using a Mattson (Alpha Centauri) Fourier transform infrared spectrometer at 4-cm^{-1} resolution using a Perkin-Elmer solution cell with CaF_2 windows and a 0.1-mm Teflon spacer. To reduce signal-to-noise, 1024 scans were coadded and triangularly apodized. Details of data acquisition are described in Trewhella et al. (1989). Spectra were analyzed by using spectral subtraction, resolution enhancement techniques of Fourier deconvolution, and second-derivative analysis, all of which are also described in Trewhella et al. (1989).

Small-Angle X-ray Scattering Data Acquisition and Analysis. X-ray scattering data were measured using the small-angle instrument described in Heidorn and Trewhella (1988). The sample-to-detector distance was 64 cm. All measurements were taken at room temperature. Scattering data were reduced to $I(Q)$ versus Q for analysis as described in Heidorn & Trewhella (1988). $I(Q)$ is the scattered X-ray intensity per unit solid angle, and Q is the amplitude of the scattering vector. ($Q = 4\pi \sin(\theta)/\lambda$, where 2θ is the scattering angle and λ is the wavelength of the scattered X-rays, λ = 1.542 Å for the CuKα used.) Guinier (1939) and the indirect Fourier transform [or $P(r)$] (Moore, 1980) analyses were used to calculate radius of gyration (R_g), forward scatter (I_0), and vector distribution functions ($P(r)$).

R_g for a homogeneous particle is the root-mean-square of the distances of all elemental scattering volumes from the center-of-mass of the particle. Guinier (1939) showed that the intensity of the innermost portion of the scattering profile can be approximated well by a Gaussian curve:

$$I(Q) = I_0 e^{-Q^2 R_g^2/3} \quad (1)$$

where I_0 is the forward, or zero angle, scatter. For globular objects the Guinier approximation is typically valid for $QR_g < 1.3$. From eq 1, it can be seen that a plot of $\ln(I(Q))$ vs Q^2 gives a straight line with slope $-R_g^2/3$ and an extrapolated intercept $\ln I_0$.

The pair-distance, or vector distribution function for a homogeneous scattering particle, $P(r)$, is the frequency of vectors connecting small-volume elements within the entire volume of the scattering particle and is calculated as the inverse Fourier transform of the scattering profile:

$$P(r) = (1/2\pi^2) \int I(Q)\, Qr \sin(Qr)\, dQ \quad (2)$$

using the indirect Fourier inversion algorithm with slit-smearing, developed by Moore (1980). The vector distribution function goes to zero at a value corresponding to the maximum linear dimension of the particle, d_{max}. R_g and I_0 can also be calculated from the second and zeroth moments of $P(r)$, respectively.

For a monodisperse solution, the volume of the scattering particle, V, can be calculated using the following relationship (Porod, 1982):

$$V = 2\pi^2 I_0 / Q_i \quad (3)$$

where Q_i is the invariant:

$$Q_i = \int_0^\infty Q^2\, dQ\, I(Q) \quad (4)$$

Modeling. A comparison was made between the $P(r)$ function for the catalytic subunit of the cAMP-dependent protein kinase/PKIα(5–22)amide binary complex obtained from small-angle scattering in this study and the previously determined crystal structure for the very similar complex (Knighton et al., 1991a) which differed only in having the slightly longer peptide PKIα(5–24) bound. Both PKIα(5–22)amide and PKIα(5–24) bind the protein kinase identically (Glass et al., 1989). A model based on the crystal structure consisting of three uniform scattering density ellipsoids was used to interpret the scattering data. This simplified model adequately matched the resolution of the scattering data and facilitated modeling the conformational changes associated with the peptide binding by dramatically decreasing computational times for testing very large numbers of models. The crystal structure was divided into three regions which could be well approximated by ellipsoids. The protein kinase catalytic subunit consists of 350 residues and has a predominantly bilobal structure: a small lobe (residues 34–125) and a large lobe (residues 126–319). The first region included residues defining the small lobe (34–125) plus the C-terminal residues 320–350 which span the surface of the small lobe. The second region included residues of the large lobe (126–319) plus the bound inhibitor peptide which interacts predominantly with the large lobe. A third region was defined by residues 15–33 of the N-terminal, which form an amphipathic α-helix that lies along the surface of the large lobe. An attempt to include these residues with the second region resulted in an ellipsoid for that region that extended beyond the molecular boundary. This gave rise to R_g values using the ellipsoid generation method discussed below that were consistently too large; hence, residues 15–33 were modeled as a third ellipsoid. The atomic coordinates of the first 14 residues were not resolved in the crystal structure, and this part of the protein is presumed to be disordered. These latter residues were therefore omitted in the model calculations (resulting in at most a 0.5 Å error in R_g).

The model ellipsoids were determined by assigning a c-axis in the direction of the longest distance vector between atomic

centers in each region with its amplitude equal to half this vector length. Similarly, the b-axis was assigned the direction of the longest distance vector between the atomic centers perpendicular to the c-axis with its amplitude equal to half this vector length. The a-axis was assigned the direction perpendicular to the b- and c-axes with an amplitude equal to half the vector length of the longest distance vector between atomic centers which lie in the plane perpendicular to the c-axis and containing the b-axis. The scattering densities of the solvent and protein components were determined from their chemical composition and respective specific volumes. The $P(r)$ function was then calculated using a Monte Carlo integration technique similar to the method described in Heidorn and Trewhella (1988). The model structure was placed in a box and random points were generated within this box. Points which hit within the molecules were saved and the $P(r)$ function was calculated from the distances between every pair of saved points. The generated $P(r)$ function is the average of 10 simulations of 4000 saved points each.

Model intensity curves were calculated from the model $P(r)$ functions using the inverse relation of eq 2:

$$I(Q) = 4\pi \int P(r) \sin(Qr)/(Qr)\, dr \qquad (5)$$

The corresponding model $P(r)$ functions were then recalculated using eq 2 and the indirect Fourier inversion algorithm (Moore, 1980) over the Q-range equivalent to that measured in the experiments. This procedure accounts for truncation effects implicit in the indirect Fourier inversion algorithm arising from the fact that the data can be measured only over a finite Q-range. These model $P(r)$ functions were compared with the $P(r)$ functions calculated from the scattering data. For comparisons of model intensity curves with the scattering data, a smearing correction was applied to the model scattering profiles to account for the slit geometry of the small-angle scattering station.

The increase in R_g and d_{max} of the protein kinase catalytic subunit that is observed upon removal of the inhibitor peptide was also modeled. The starting parameters for the model were based on the atomic coordinates obtained from the crystal structure of the binary complex, but with the inhibitor peptide omitted. Inspection of the crystal structure reveals that the large and small lobes of the kinase are connected by an extended peptide chain region formed by residues 120–128 that could act as a hinge deep in the cleft between the two lobes. This cleft also contains the MgATP-binding site and the residues involved in phosphotransferase activity. Further, glycine residues (Gly 125 and Gly 126) are optimally located in this interconnecting region, suggesting points of potential flexibility at which a molecular hinge can be defined. The only other part of the polypeptide chain that spans between both domains is a short C-terminal segment (residues 307–330). This segment also contains a glycine residue (Gly 320) that is located ≈7 Å from Gly 125 in a direction away from the binding cleft. Gly 125, Gly 126, and Gly 320 were identified as points of potential flexibility in the structure. Various hinges and hinge orientations in the vicinity of these residues were defined and experimented. Attempts to model the opening of the structure upon removal of the inhibitor peptide using Gly 320 as the hinging point consistently gave poor agreement with the observed data. In addition, hinge motions involving Gly 320 generally resulted in the structure breaking apart at residues 125 and 126 in the other connecting strand between the two lobes. Inspection of the structure reveals why this hinge would cause the structure to break; it is in part a consequence of the fact that Gly 320 is positioned more distant from the binding cleft compared with Gly 125.

Hinges involving Gly 125 were also experimented with. The hinge that showed the more favorable characteristics, including the least problems with steric crowding, was defined perpendicular to the α-carbons of Gly 125 and Gly 126 and was positioned so it passed through the α-carbon of Gly 125. Importantly, opening the structure using this hinge mechanism did not result in a breaking apart of the structure at Gly 320, which only moved ≈3 Å from its starting position for the "open" model that best fit the data. The model that best fit the scattering data was identified by a search in which residues defining the small lobe (34–125) plus the C-terminal residues (320–355) were rotated at 1° increments from 0° to 90°. Residues 15–33 were also allowed to rotate along with the small lobe since they are contiguous with that polypeptide segment. The $P(r)$ function for each structure so generated was calculated by the same method as done for the peptide-bound structure, i.e., by defining the three-ellipsoid model for the rotated structure and using the Monte Carlo integration technique. The residues included within the three regions that defined each ellipsoid were the same as for the model of the peptide bound complex, but with the peptide omitted. Each $P(r)$ function generated was the result of 4000 saved points. From this set, the model that gave the same R_g and d_{max} as the scattering data was chosen. For detailed comparison with the $P(r)$ function derived from the scattering data, the statistics of the model $P(r)$ were improved by averaging the results of 10 simulations, each with 4000 saved points.

RESULTS

FTIR Spectroscopy. Resolution enhanced FTIR spectra of the cAMP-dependent protein kinase catalytic subunit alone, and of the protein kinase plus PKIα(5–22)amide, and the second derivatives of these spectra are shown in Figure 1. Secondary structure composition was determined for each on the basis of the frequency assignments of the amide I′ bands resolved in the Fourier deconvolved spectra (Byler & Susi, 1986; Reed et al., 1989). These frequency assignments are given in Table I, together with the corresponding relative intensities as a percentage of the total intensity in the amide I′ region. Also shown in Table I is a summary of the percentages of each secondary structural element estimated from the FTIR spectra compared with values determined for the protein kinase/inhibitor peptide complex from the crystal structure (Knighton et al., 1991a). The values for the crystal structure were taken from the analysis provided by Knighton et al. (1991a), as well as by inspection of the crystal structure using TOM-FRODO (Jones, 1978; Cambillau & Horjales, 1987) on a Silicon Graphics workstation. The β-turn/bend content was established by examining turn structures and measuring H-bond lengths, torsion angles, and overall geometry. The agreement between the FTIR results and the crystal structure is quite good, the largest discrepancy being for the turn/bend structures. Since the crystal structure is relatively low resolution (2.7 Å), this discrepancy is not surprising. Indeed, as is usually the case at this level of resolution, there are a number of unphysical torsion angles in the crystal structure model.

No significant difference was observed in the FTIR deconvolved spectra for the protein kinase in the presence or absence of inhibitor peptide (Figure 1). The peptide itself is small (5% of the total structure) and has several of the major structural elements present in the protein kinase (≈30% α-helix plus one β-turn (Reed et al., 1989)), and hence it is not expected

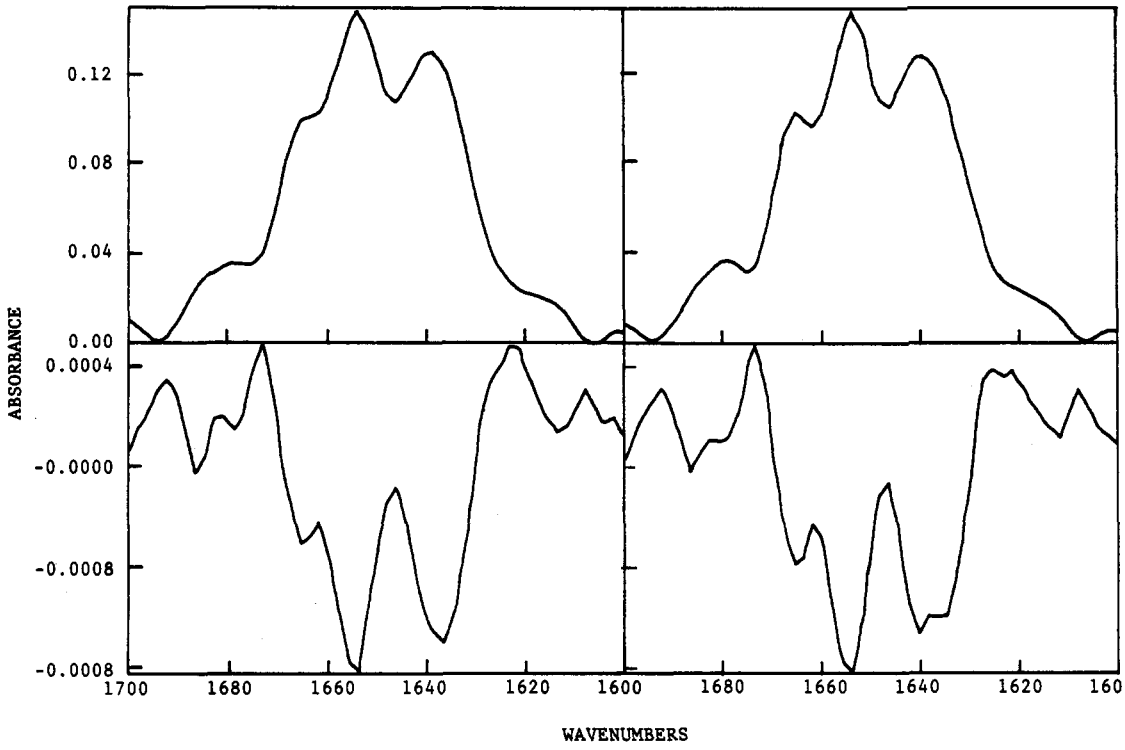

FIGURE 1: Top: Resolution-enhanced (by Fourier deconvolution) buffer subtracted FTIR spectrum for the catalytic subunit of the cAMP-dependent protein kinase (left) and for protein kinase plus equimolar PKIα(5–22)amide (right). Bottom: Corresponding second-derivative spectra.

Table I

A. Peak Positions (in cm^{-1}) and Intensities[a] (as % of Total)

assignment	extended/ β	extended/ β	α-helix	β-turn/ bend	extended/ β
protein kinase	1619 (6.1%)	1636 (30.1%)	1651 (34.2%)	1666 (21.3%)	1682 (8.2%)
protein kinase plus PKI-(5–22)-amide	1620 (6.2%)	1635 (29.5%)	1652 (34.3%)	1665 (21.9%)	1683 (8.0%)

B. Comparison[b] of Secondary Structure

	extended/ β-strand	helix	β-turn/bend	unknown
crystal structure	49%	33%	14%	4%
FTIR spectrum	44%	34%	22%	

[a] The peak positions and intensities are for components in the amide I′ region of the FTIR spectra for the catalytic subunit of the cAMP-dependent protein kinase with and without PKI(5–22)amide. [b] The secondary structure comparison is between that determined by FTIR and that from the crystal structure of the catalytic subunit of the cAMP-dependent protein kinase plus inhibitor peptide.

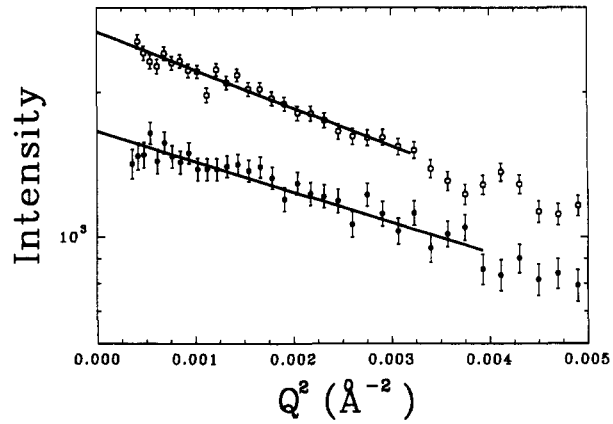

FIGURE 2: Guinier plots of X-ray scattering data for the catalytic subunit of the cAMP-dependent protein kinase with (●) and without (○) PKIα(5–22)amide. The samples are 0.066 mM protein in 10% glycerol and 27.2 mM MES buffer in H_2O.

to influence the percent structural elements greatly. The calculated percentage secondary structure for the protein kinase alone as determined by the FTIR measurements (Table I) agrees well with two of three previous reports for the measurement of secondary structure of the protein kinase determined by circular dichroism. (Sugden et al., 1976; Ul'masov et al., 1981; Reed & Kinzel, 1984). The FTIR data indicate that the secondary structure of the cAMP-dependent protein kinase catalytic subunit is not significantly altered by the binding of PKIα(5–22)amide.

Small-Angle X-ray Scattering Data. Scattering data collected for the protein kinase in 5% glycerol showed significant aggregation as evidenced by nonlinear Guinier plots in the region $Q = 0.007$–0.06 Å^{-1}, indicating that some of the scattering particles have R_g values greater than $\approx$150 Å. Increasing the glycerol content to 10% (w/v) eliminated the aggregation, provided the protein concentration was $\leq$0.07 mM. Initially, the glycerol was kept in the samples because it has been well established as a means to stabilize the protein and maintain its specific activity during storage. Samples with glycerol can be stored for several months without problems, whereas without it activity rapidly diminishes within days. Figure 2 shows Guinier plots calculated for the protein kinase catalytic subunit (0.066 mM) in 10% glycerol, with and without equimolar concentrations of the inhibitor peptide PKIα(5–22)amide. Samples measured gave Guinier regions that could be fit with a single straight line with reduced values $\chi^2 \approx 1$ and no evidence of upward curvature at low Q. As expected for monodisperse solutions, there is good agreement between the values obtained using the Guinier and the $P(r)$ analyses (Table IIA). The structural parameters in Table IIA were calculated from the combined data of a series of scattering experiments using three samples of protein kinase and two samples of protein kinase plus peptide, all made using

Table II: Structural Parameters

A. Parameters from the X-ray Scattering Data

	Guinier analysis		P(r) analysis			
	R_g (Å)	χ^2	R_g (Å)	d_{max} (Å)	V (Å^3)	χ^2
protein kinase	23.1 ± 0.5	1.00	23.0 ± 0.4	73 ± 3	52983 ± 2791	1.27
protein kinase plus PKI-(5–22)amide	21.1 ± 0.8	0.81	21.0 ± 0.4	62 ± 3	52278 ± 6324	0.96

B. Parameters[a] for the Three-Ellipsoid Models

	R_g (Å)	d_{max} (Å)	χ^2
protein kinase	23.0	72	1.29
protein kinase plus PKI(5–22)amide	21.1	63	0.94

[a] The model R_g and d_{max} values are calculated from the respective model $P(r)$'s. Reduced χ^2 for the model calculations given were calculated from slit-smeared intensity curves of the models compared with measured intensity curves.

a single preparation of protein kinase. The volumes calculated from these data, using eqs 3 and 4, were consistent with those expected for scattering from monodisperse samples of the 40 862-Da protein and also with the dimensions obtained from the crystal structure (Knighton et al., 1991a). These data show that the addition of inhibitor peptide to the protein kinase results in a 2-Å decrease in R_g and an 11-Å decrease in d_{max}. Additional measurements were made using samples from independent protein kinase preparations, and the 2-Å decrease in R_g was consistently observed for the protein kinase upon peptide addition, although at higher concentrations (5–7 mg/mL) slight aggregation generally occurred and the structural parameters were consequently systematically increased.

Modeling the Structures. Figure 3 shows the X-ray scattering data, $I(Q)$ vs Q, for the protein kinase/inhibitor peptide complex and its associated $P(r)$ function. Also shown are the calculated scattering profile and $P(r)$ function for the three-ellipsoid model of the binary complex (described in Materials and Methods). The model gives a very good fit to the scattering data (Table IIA), with a reduced χ^2 of 0.94 (Table IIB). Figure 4 shows the X-ray scattering data for the protein kinase without the inhibitor peptide and its associated $P(r)$ function. Since the FTIR data show the secondary structure of the protein kinase to be unchanged in the presence of the inhibitor peptide, the changes in R_g and d_{max} observed by X-ray scattering in the presence versus absence of the inhibitor peptide were modeled as changes in the spatial relationship between the lobes of the protein kinases. The overall dimensions of each lobe and their secondary structure were assumed to be invariant at the resolution of the scattering experiment. The 2-Å increase in R_g and 11-Å increase in d_{max} observed upon removal of the inhibitor peptide indicate an elongation of the structure. One mechanism that could account for these changes would be the opening of the cleft between the small and large domains of the structure that contains many of the elements of the catalytic site. Therefore, a molecular hinge was defined deep in the cleft between the two domains such that the two domains could be rotated with respect to one another (see Materials and Methods). Similar bivalve-like hinge mechanisms have been well documented with other enzymes (Knowles, 1991).

Figure 5 shows the dependence of R_g and d_{max} for the structure upon rotation of the two lobes with respect to each other about this hinge in 1° increments. A rotation of 39° gave R_g and d_{max} values matching those obtained experimentally for the protein kinase in the absence of the inhibitor peptide (Table II). However, since a large rotation of the small lobe results in a relatively small change in R_g, the error

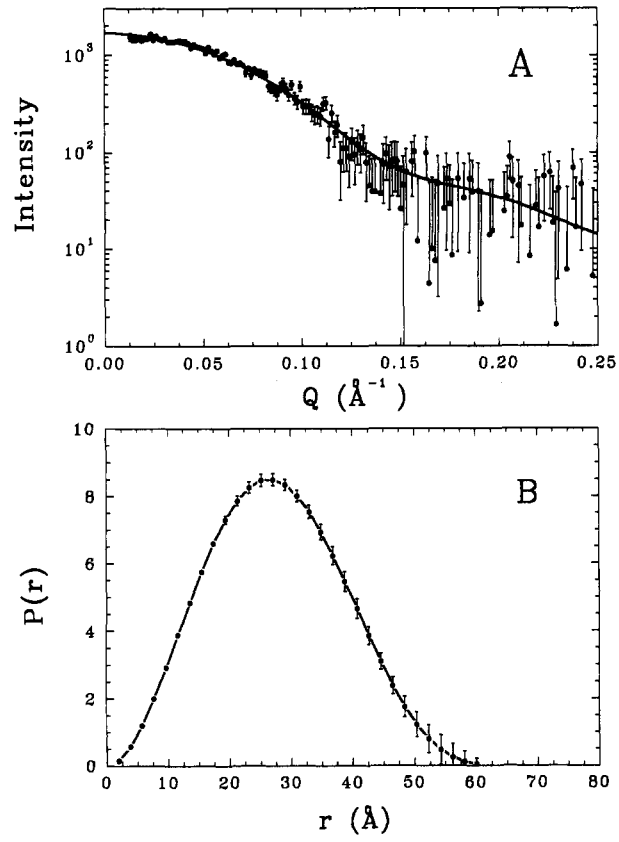

FIGURE 3: Top: Comparison of X-ray scattering data for 0.066 mM protein kinase plus equimolar PKIα(5–22)amide in 10% glycerol and 27.2 mM MES buffer in H_2O (●) with that calculated from the three-ellipsoid model (—). The coordinates used in the model calculation are taken from Knighton et al. (1991a) and the structure is as shown in Figure 6 (top). The results of the model fits are given in Table IIB. Bottom: $P(r)$ functions corresponding to the above intensity curves. The Q-range used in the $P(r)$ analysis was 0.017–0.22 Å^{-1}. The χ^2 for the $P(r)$ analysis of the measured data was 0.96 (for 129 degrees of freedom).

in the experimentally measured R_g would not preclude rotations in the range of 27–58°. The calculated scattering profile and $P(r)$ function derived from the model structure generated by rotating the two lobes 39° are also shown in Figure 4, and a summary of the structural parameters is given in Table IIB. This "open" structure shows an excellent fit to the scattering data giving a reduced χ^2 of 1.29. This hinge orientation and degree of rotation is also appealing because steric crowding of atoms resulting from the movement of the domains remained low, increasing only about 5% relative to the original crystal structure. This was checked by defining Van der Waals spheres around each atom in the model structure and determining the number of overlapping atoms. A loop region which includes a β-turn is located in the small lobe between residues 98 and 108. This loop region is located on the back side of the small lobe opposite to the inhibitor peptide binding site and makes contact with the large lobe by interacting with an α-helix (residues 150–160) and an extended region (residues 180–190) which flanks the α-helix. The hinge motion chosen resulted in the base of this loop remaining fairly stationary while other hinges resulted in this loop crowding into atoms in the large lobe. This hinge motion also resulted in the α-helix at the N-terminal (residues 15–33) rotating slightly which gave rise to a small amount of steric crowding with respect to the large lobe. This could easily be reduced by allowing this helix to rotate about its point of attachment to the small lobe, but considering the limited resolution of scattering data, the model was not further refined.

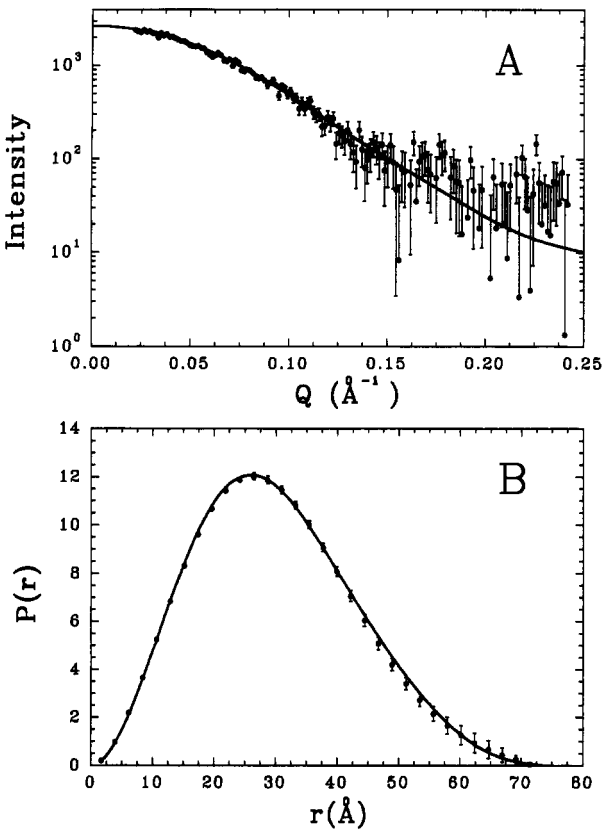

FIGURE 4: Top: Comparison of scattering curves for the catalytic subunit of cAMP-dependent protein kinase (0.066 mM, without PKI peptide) in 10% glycerol and 27.2 mM MES buffer in H_2O (●) with that calculated from the model (—). A molecular hinge was defined whereby the two lobes of the protein could rotate about one another. The hinge was located deep in the cleft between the two lobes and it was oriented perpendicular to the α-carbons of Gly 125 and Gly 126 and passed through the α carbon of Gly 125. Results of this model are given in Table IIB. The model required a 39° rotation of the two lobes with respect to each other in order to effect the increase in R_g and d_{max} from the known inhibitor peptide bound form to the free form. The coordinates for this model are depicted in Figure 6 (bottom). Bottom: $P(r)$ functions corresponding to the above intensity curves. The Q-range used in the $P(r)$ analysis was 0.02–0.22 Å^{-1} with four coefficients. The χ^2 for the $P(r)$ analysis of the measured data was 1.27 (for 126 degrees of freedom).

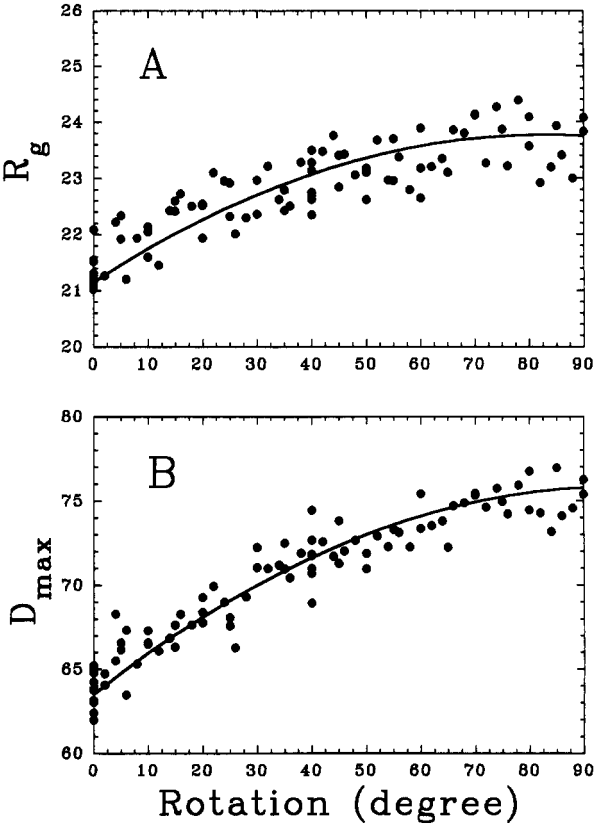

FIGURE 5: R_g and d_{max} calculated for every degree of rotation of the small and large lobe of the catalytic subunit of protein kinase. The small lobe of the protein kinase is rotated with respect to the large lobe by defining a molecular hinge as described in the caption of Figure 4. The data points are scattered due to the randomness associated with the Monte Carlo integration technique used in the calculation. The solid lines in each graph are a least-squares polynominal fit to the data. From this fitted curve, a rotation of 39° is required to match R_g and d_{max} to the experimental values.

It should be stressed here that the search for a model to fit the experimental data for the "open" structure without peptide bound was not a totally unconstrained search of all conformational space. Solution scattering data can never prove a single model correct, since the data are spherically averaged because of the random orientations of molecules in solution. However, one can test models based on other data. We have utilized the crystal structure data and the optimal locations of glycines residues which are known to be able to provide points of flexibility for hinge-type motions. We have also applied constraints such as avoiding severe steric crowding and requiring the polypeptide to remain contiguous. The model presented here is appealing in that it shows the small lobe of the kinase lifting off the large lobe exposing the peptide binding site. The details of the opening of the cleft may be more complex than a simple hinge motion as in our model, but this model has all the necessary elements to make it plausible.

By all the criteria discussed the proposed hinging of the protein kinase structure at Gly 125, with a rotation of 39° induced by inhibitor peptide binding, provides an excellent fit to the experimental data. A stereodrawing of the polypeptide backbone for the protein kinase plus peptide (taken from the crystal structure) and the proposed model for the inhibitor peptide free protein kinase are shown in Figure 6. For clarity only the α-carbons are presented. The data presented strongly support the proposal that in the absence of inhibitor peptide the protein kinase assumes an open configuration illustrated with a wide opening of the cleft that contains the catalytic site. Upon inhibitor peptide binding this cleft collapses toward the peptide leading to the closed conformation seen for the binary complex in the crystal structure and in solution.

DISCUSSION

The peptides derived from the protein kinase inhibitor, PKI, mimic the interactions of protein substrates with the protein kinases catalytic site (Walsh et al., 1990), and the binding of either involves many of the same determinants. Of note, no substrate maximizes the interactions with the protein kinase to the extent that occurs with PKI. None of the cAMP-dependent protein kinase substrates yet identified contain a phenylalanine within an amphipathic α-helix at position P-11, which is important for the optimum binding of PKI. [Nomenclature for protein kinase substrates is according to Knighton et al. (1991b).] In substrates, there is a marked variation in the location and nature of basic residues at residues P-1 to P-6. In addition, the hydrophobic isoleucine, that is essential at P+1 in PKI for maximum binding, shows marked variation in substrates even to the extent that in some it is replaced by an acidic residue. It appears, in fact, that protein substrates may have evolved to varying degrees to the extent

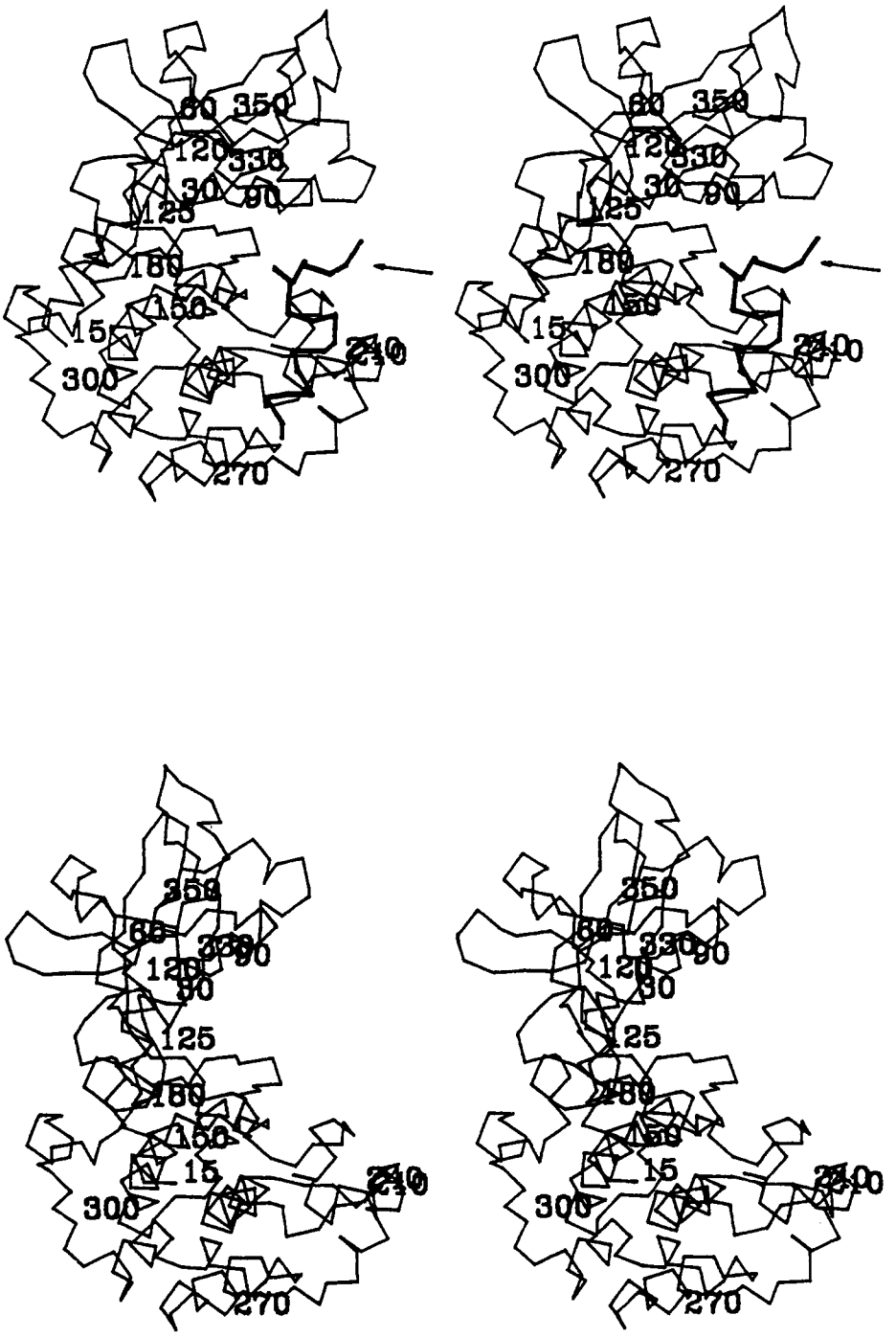

FIGURE 6: Stereodrawings of the cAMP-dependent protein kinase catalytic subunit with PKIα(5–24) (top), taken from Knighton et al. (1991a), and the proposed model for the protein kinase alone (bottom). Only the α-carbon trace is shown and every 30 residues are labeled for clarity. The inhibitor peptide in the binary complex is indicated by the bold line and by the arrow. The two depicted structures have the same orientation with the molecular hinge perpendicular to the plane of the page and passing through the α-carbon of Gly 125 which is also labeled.

that they mimic the binding interactions that occur with PKI and that there may in fact be a physiological hierarchy of substrate efficacy (Walsh et al., 1992). To date, the synthetic substrate (Ser 21)PKIα(14–22)amide exhibits a lower K_m and a higher k_{cat} than for any other substrate identified for this enzyme (Glass et al., 1989). PKI thus appears to bind with optimum efficiency to the protein kinases catalytic site. There is a very good likelihood that the conformational changes induced in the protein kinase catalytic subunit upon PKI binding will also occur with protein substrates. However, given that these substrates do not bind with as high affinity as does PKI, it is also likely that there will be often subtle but important differences in the changes induced by different protein substrates. In fact, this may allow the catalytic site to accommodate protein substrates of different dimensions and spatial arrangements.

The effects of the PKI peptide on the conformation of the c-AMP-dependent protein kinase described here are similar to those identified for several substrate–enzyme interactions (Knowles, 1991). Hexokinase is one close example. Like the protein kinase catalytic subunit, it is a bilobal protein and the binding of the substrate glucose results in a closure of the cleft between the two lobes. This places the glucose moiety in close proximity to the residues of the enzyme involved in catalysis and the bound ATP, and it also excludes water from the catalytic site (Bennett & Steitz, 1978; McDonald et al.,

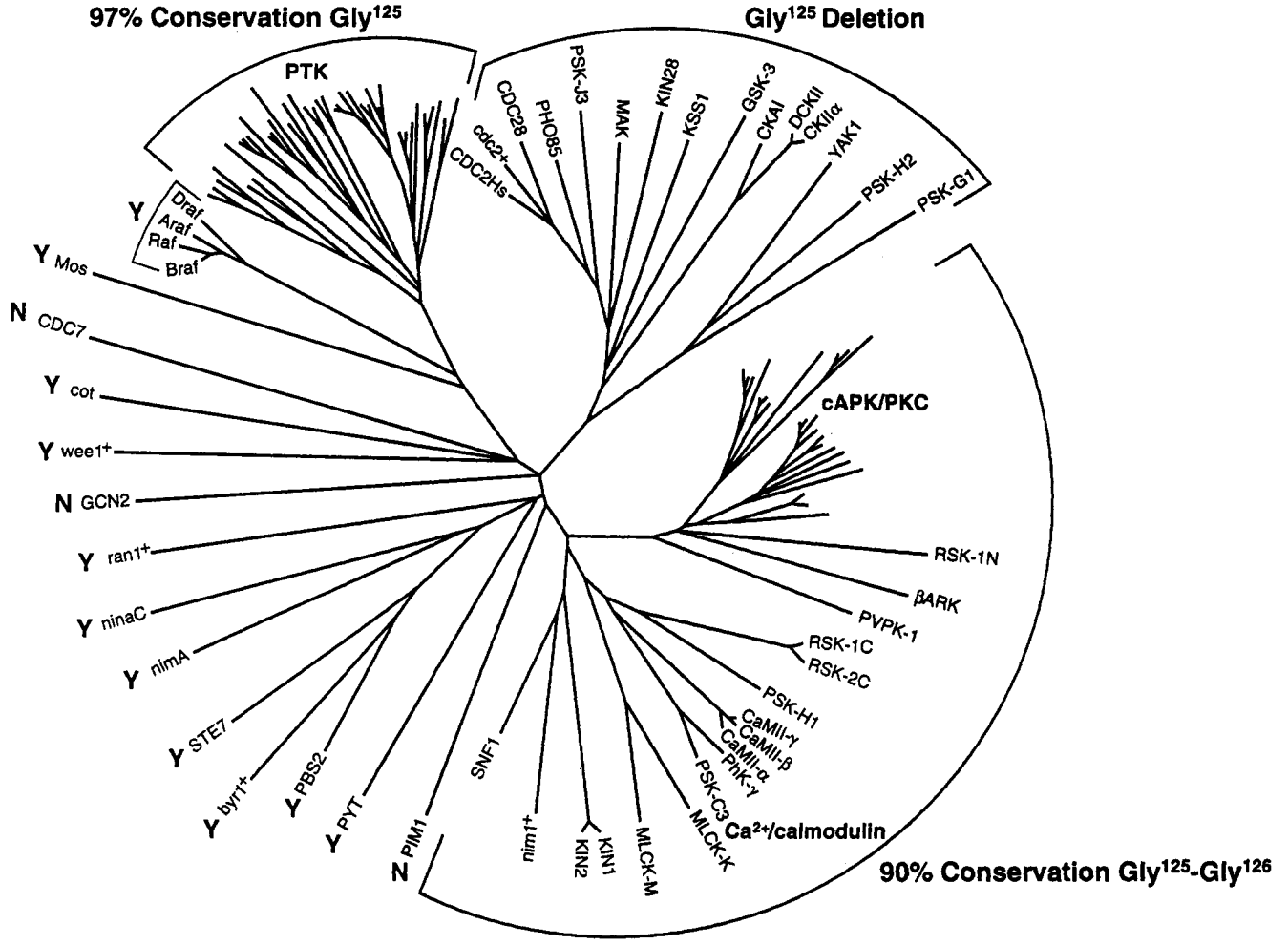

FIGURE 7: Conservation of the Gly 125 residue of the cAMP-dependent protein kinase in other members of the protein kinase gene family. The phylogenetic tree is taken from Hanks & Quinn (1991) and shows 115 of the 205 members of the gene family now in the data bank (Hanks & Quinn, 1991). Listings of the specific members of the PTK (protein tyrosine kinase) and cAPK/PKC (cAMP protein kinase/protein kinase C) branches and the definition of the abbreviations of the other protein kinases are given in Hanks and Quinn (1991). Of the 205 members of the current data bank, 59 belong to the cAMP pair of glycines equivalent to Gly 125/126 and the other six have a single Gly 125 equivalent. Of the 73 current members of the PTK family, 62 have a single glycine and 8 have a pair of glycines in the Gly 125 position. Of the 36 current members of the cdc2 kinase/casein kinase/GSK-3 kinase branch, none have a glycine equivalent to the Gly 125 position. Of the remaining 27 kinases of the data bank, 14 have a single glycine, 3 have a double glycine (both indicated by Y), and 10 do not have a glycine in the Gly 125-equivalent position (indicated by (N)).

1979). As is proposed here for the protein kinase, this substrate-induced bivalve-like closure of the cleft of hexokinase is accomplished with the secondary structure of the protein remaining unchanged and is simply the consequence of movement of the two lobes about the flexible linkage of the interconnecting chains. What provokes these proposed changes in the protein kinase structure upon binding of PKI peptide remains to be resolved; however, inspection of the structure suggests some interesting possibilities. Most of the interactions of the residues of PKI/peptide are with amino acids in the large lobe of the protein kinase, fairly separated from the interconnecting links between the two lobes. Glu 127, however, the residue immediately adjacent to the proposed hinge at Gly 125/126, is one of the docking determinants of arginine at P-3 in PKI. This arginine also interacts with Asp 229 and Glu 231, both of which are on the small lobe side of the flexible linkage glycines of the C-terminal chain of the kinase. One, more, or all of these interactions might be the trigger that causes the rotation at the closely neighboring glycines of the two linkage chains. This arginine is also one of the key determinants of protein kinase substrates and thus, if this is the mechanism that prompts the conformational change, substrates would do likewise. With PKI peptides, there is also a fairly close topographical relationship between the amphipathic amino terminal helix of residues P-10 to P-16 of PKI and α-helix D of the protein kinase that spans from residues 128 to 135 and is immediately adjacent to the proposed hinge at Gly 125/126. An interaction between these two helices might influence the rotation of the lobes. If so, this would be an interaction not shared with protein substrates.

The cAMP-dependent protein kinase is one of a family of 205 protein kinases (Hanks & Quinn, 1991), and it is to be expected that they would share between them some of the same features of enzyme catalysis. The conservation of the glycine equivalent to that of Gly 125 of the cAMP-dependent protein kianses has a very distinctive pattern (Figure 7). In the cAMP-dependent protein kinase, Gly 125 is one of a pair of contiguous glycines, and this property is shared by 53 out of 59 enzymes in the cAMP-dependent protein kinase/protein kinase C/Ca^{2+} calmodulin-dependent phylogenetic group of kinases, with the remaining six kinases of this group having a single glycine, for a 100% overall conservation of the single glycine at the Gly 125-equivalent position. A single glycine at this position is also conserved in 96% (70/73) of identified protein tyrosine kinases. In contrast to this very high degree of conservation in two of the more diverse phylogenetic

branches of the kinase gene family, none of the 36 kinases in the cdc2 kinase/casein kinase/GSK-3 kinase group contained a glycine at a position equivalent to Gly 125. Further, sequence alignment (Hanks & Quinn, 1991) suggests that a two amino acid deletion has occurred at this position. The very high degree of conservation in these two groups of kinases (and a 71% conservation overall) demonstrates the importance of Gly 125 and provides corollary support for its proposed role as the site of conformational rotation. Its absence from one branch of the kinase gene family suggests that in those protein kinases an alternate mode of cleft cleavage has been adopted. Alternatively, the three-dimensional structure and topography of the group of proteins phosphorylated by these enzymes does not require cleft closure.

ACKNOWLEDGMENT

We thank Christian Brun for technical assistance in the reduction and analysis of X-ray scattering data.

REFERENCES

Bennett, W. S., Steitz, T. A. (1978) *Proc. Natl. Acad. Sci. U.S.A. 75*, 4848–4852.

Byler, D. M., Susi, H. (1986) *Biopolymers 25*, 469–487.

Cambillau, C., & Horjales, E. (1987) *J. Mol. Graphics 5*, 174–177.

Fletcher, W. H., Van Patten, S. M., Cheng, H.-C., & Walsh, D. A. (1986) *J. Biol. Chem. 261*, 5504–5513.

Glass, D. B., Cheng, H.-C., Mueller, L. M., Reed, J., & Walsh, D. A. (1989) *J. Biol. Chem. 264*, 8802–8810.

Guinier, A. (1939) *Ann. Phys. (Paris) 12*, 161.

Hanks, S. K., & Quinn, A. M. (1991) *Methods Enzymol. 200*, 38–62.

Hanks, S. K., Quinn, A. M., & Hunter, T. (1988) *Science 241*, 42–52.

Heidorn, D. B., & Trewhella, J. (1988) *Biochemistry 27*, 909.

Knighton, D. R., Zheng, J., Ten Eyck, L. F., Ashford, V. A., Xuong, N., Taylor, S. S., & Sowadski, J. M. (1991a) *Science 253*, 407–414.

Knighton, D. R., Zheng, J., Ten Eyck, L. F., Xuong, N., Taylor, S. S., & Sowadski, J. M. (1991b) *Science 253*, 414–420.

Knowles, J. J. (1991) *Nature 350*, 121–124.

Jones, T. A. (1978) *J. Appl. Crystallogr. 11*, 268.

McDonald, R. C., Steitz, T. A., & Engelman, D. M. (1979) *Biochemistry 18*, 338–342.

Mitchell, R., Sosnick, T. R., Glass, D., Walsh, D. A., & Trewhella, J. (1990) *Biophys. J. 57*, 429a.

Moore, P. B. (1802) *J. Appl. Crystallogr. 13*, 168.

Porod, G. (1982) in *Small Angle X-ray Scattering*, pp 17–51, Academic Press, New York.

Reed, J., & Kinzel, V. (1984) *Biochemistry 23*, 1357–1362.

Reed, J., de Ropp, J. S., Trewhella, J., Glass, D. B., Liddle, W. K., Bradbury, E. M., Kinzel, V., & Walsh, D. A. (1989) *Biochem. J. 264*, 371–380.

Sugden, P. H., Holladay, L. A., Reimann, E. M., & Corbin, J. D. (1976) *Biochem. J. 159*, 409–422.

Trewhella, J., Lidle, W. K., Heidorn, D. B., & Strynadka, N. (1989) *Biochemistry 28* (3), 1294–1301.

Ul'masov, K. A., Nesterova, M. V., Poletaev, A. I., & Severin, E. S. (1981) *Biokhimiya (Moscow) 46*, 1609–1614.

Van Patten, S. M., Ng, D. C., Th'ng, J. P. H., Angelos, K. L., Smith, A. J., & Walsh, D. A. (1991) *Proc. Natl. Acad. Sci. U.S.A. 88*, 5383–5387.

Van Patten, S. M., Howard, P., Walsh, D. A., & Maurer, R. A. (1993) *Mol. Endocrinol.* (submitted for publication).

Walsh, D. A., Angelos, K. L., Van Patten, S. M., Glass, D. B., & Garetto, L. P. (1990) The Inhibitor Protein of the cAMP-dependent Protein Kinase, in *Peptides and Protein Phosphorylation* edited by (Kemp, B. E., Ed.) pp 43–84, CRC Press, Boca Raton, FL.

Walsh, D. A., Glass, D. B., & Mitchell, R. (1992) *Curr. Opin. Cell Biol. 4*, 241–251.